Sonochemistry-assisted Fabrication of 1D-ZnSb$_2$O$_6$@2D-MoS$_2$ Nanostructures: a Synergistic Energy Storage Material for Supercapacitors

M. Balasubramaniam[1], Smagul Karazhanov[2] and S. Balakumar[1,*]

[1]National Centre for Nanoscience and Nanotechnology, University of Madras, Guindy campus, Chennai-600 025, India.
[2]Solar Energy Department, Institute for Energy Technology (IFE), Kjeller, Norway.

*Email: balasuga@yahoo.com

Abstract

In this work, a novel nanohybrid composing of molybdenum disulphide nanosheets and zinc antimonate nanorods was fabricated using ultrasonication assisted homogenous magnetic stirring approach and investigated their electrochemical performance as an electrode material for supercapacitors. First and foremost, the fabricated nanohybrid electrode material was investigated through XRD, FT-IR, FE-SEM, HR-TEM, UV-DRS and XPS to determine their structural, vibrational, morphological, optical and chemical compositional characteristics. Subsequently, the electrochemical properties of the nanohybrid electrode were explored using CV, GCD and EIS studies in 1.0 M KOH solution. The fabricated nanohybrid electrode material exhibited tremendous electrochemical performance by distributing maximum specific capacitance of 469.28 F g^{-1} at a current density of 5.0 A g^{-1} with high cycling stability of 102.0% even after 2000 cycles at a current density of 10.0 A g^{-1}. These exceptional electrochemical characteristics of MoS$_2$/ZnSb$_2$O$_6$ nanocomposites are ascribed to the influence of ultrasonication on non-aggregated nanocomposite formation, existence of more number of electrochemical active sites and synergistic interactions between two different nanostructures. The acquired results confirmed that MoS$_2$/ZnSb$_2$O$_6$ nanocomposites could be a prospective and electrochemically active candidate as electrode materials for supercapacitors.

Keywords: Molybdenum disulphide nanosheets; zinc antimonate nanorods; ultrasonication; synergistic interactions**;** electrochemically active; supercapacitors.

1. Introduction

Recently, two-dimensional transition metal dichalcogenides (TMDs) such as, molybdenum disulfide (MoS$_2$) have attracted much attention in electrochemical capacitors [1-4], owing to their distinct chemical and structural properties. MoS$_2$ possess layered hexagonal structure involving covalently bonded S-Mo-S, which is separated by a relatively weak van der Waals force [5, 6]. Therefore, it is reliable to separate individual MoS$_2$ layers from their bulk counterparts [7, 8]. On the other hand, MoS$_2$ typically reveals extremely low conductivity that would appreciably repress their overall electrochemical performance [9]. Additionally, the prepared MoS$_2$ layers would easily re-stack and aggregate, which could lead to reduced specific active surface area, thereby, reduced specific capacitance [10]. Moreover, due to stacking, ion transport rate can also be reduced that can hinder the overall electrical conductivity, thus, leading to rapid capacitance fading and inferior rate capability [11]. Therefore, avoiding the stacking and aggregation effects can increase the electrical or ionic conductivity. In order to overcome this issue, rational design and synthesis of MoS$_2$-based nanocomposites is an effective approach for preventing stacking and aggregation of two-dimensional (2D) layers.

Very few reports have been presented on metal oxide-incorporated MoS$_2$-based nanocomposites as electrode materials for supercapacitors. Dewei Liang *et al*. [12] prepared Co$_3$O$_4$/MoS$_2$ nanocomposites, which exhibited battery-type phenomena with a maximum specific capacity of 69 mAh g^{-1} and 87.0% capacity retention after 500 cycles in 1.0 M KOH solution. Lin Ma *et al*. [13] synthesized SnO$_2$/MoS$_2$ nanocomposites and achieved a maximum specific capacitance of 159.22 F g^{-1} with 93.0% capacitance retention after 1000 cycles in 1.0 M Na$_2$SO$_4$ solution. Yukti Arora *et al*. [14] prepared MoS$_2$/BiVO$_4$ nanocomposites, which provided remarkable specific capacitance of 610 F g^{-1} with 80.0% capacitance retention after 200 cycles in 2.0 M NaOH electrolyte. Na Li *et al*. [15] prepared CeO$_2$/MoS$_2$ nanocomposites and achieved a maximum specific capacitance of 90 mF cm^{-2} with 98.0% capacitance retention, after 2000 cycles in 1.0 M Na$_2$SO$_4$ electrolyte.

To the best of author's literature knowledge, no evident reports on MoS$_2$/ZnSb$_2$O$_6$ nanocomposites as electrode materials for supercapacitors were found. Therefore, in the current investigation, ZnSb$_2$O$_6$ nanorods were anchored onto MoS$_2$ nanosheets to form MoS$_2$/ZnSb$_2$O$_6$ nanocomposites. By incorporating the ZnSb$_2$O$_6$ nanorods into 2D MoS$_2$ nanosheets, the ZnSb$_2$O$_6$ nanorods can serve as spacers to thwart the restacking of adjoining MoS$_2$ nanosheets. Additionally,

the resulting nanocomposites can greatly exhibit improved electrical conductivity and electrochemical performance that were discussed in later sections in detail.

2. Experimental

2.1. Materials

Molybdenum disulfide (<2 μm, Sigma-Aldrich), zinc acetate dihydrate $(Zn(CH_3COO)_2.2H_2O$, Merck), antimony trichloride $(SbCl_3$, Alfa Aesar), double-distilled (DD) water, and N-methyl-2-pyrrolidone (NMP) were used for the synthesis of MoS_2 and its nanocomposites.

2.2. Synthesis of Base Materials and Nanocomposites

First, required volume of N-methyl-2-pyrrolidone is taken and to that 250 mg of bulk MoS_2 powder was added, which is stirred for 1 h to obtain a homogenous solution followed by ultrasonication for 1 h in a probe-assisted ultrasonicator (PKS 250FM, PCI Analytics, 250 W, 20 kHz). Then the dispersions were ultracentrifuged at 10,000 rpm for 15 min, thereafter, the supernatant was poured away and the remaining powder was dried at 100 °C for 3 h in a hot air oven to obtain MoS_2 nanosheets. Second, $ZnSb_2O_6$ (ZSO) nanorods were synthesized by simple precipitation method [16] using zinc acetate and antimony trichloride in 250 mL aqueous media. The solution was stirred for 2 h, thereafter, a white precipitate occurred that was filtered, washed several times with DD water, and dried in hot air oven at 100 °C for 6 h. Subsequently, it was annealed at 700 °C for 4 h.

Then, the MoS_2 and $ZnSb_2O_6$ nanostructures were mixed using ultrasonication-assisted magnetic stirring approach in order to fabricate hybrid nanocomposites in the weight ratio of 1:1 and 1:2. In addition, the weight ratio of MoS_2 is increased by two parts than the weight ratio of $ZnSb_2O_6$ (i.e., 2:1) to prepare the third component. For convenience, the samples were designated hereafter as MoS_2/ZSO1 (1:1), MoS_2/ZSO2 (1:2), and MoS_2/ZSO3 (2:1), respectively. The composites were prepared by redispersing MoS_2 and ZSO separately in DD water by probe ultrasonication for 2 min each. After that, the suspensions were mixed altogether as a single mixture that was magnetically stirred for 2 h to obtain the homogenous mixture of MoS_2/ZSO nanocomposites. The crucial role of ultrasonic waves is to well disperse the ZSO nanorods and MoS_2 nanosheets to promote Brownian motion and moreover, during the preparation of the nanocomposites, the interaction of MoS_2 nanosheets and $ZnSb_2O_6$ nanorods will be synergistic.

2.3. Characterizations

The structural properties of the MoS_2 nanosheets and MoS_2/ZSO nanocomposites were studied through X-ray Diffraction (XRD) recorded using Rigaku X-ray Diffractometer consisting of Cu-$K_{\alpha 1}$ radiation (λ = 1.5406 Å) source and the patterns were recorded at a scan rate of 2°/min with an operating current and voltage at 20 mA and 40 kV, respectively. The vibrational properties of the MoS_2/ZSO nanocomposites were studied through Fourier transform infrared spectroscopy (FT-IR) analysis and the spectra were recorded using a JASCO-4100 FT-IR instrument in the range from 4000 to 400 cm^{-1}. To view the morphology, Hitachi SU-6600 based field emission scanning electron microscope (FE-SEM) at an operating voltage of 15 kV and high resolution transmission electron microscopy at an operating voltage of 250 kV (HRTEM - Tecnai 30 G^2 S-TWIN) was used and the micrographs were imaged. The UV-Visible DRS spectra of bare MoS_2 nanosheets and MoS_2/ZSO nanocomposites were recorded using JASCO-V650 Spectrophotometer within the wavelength range of 200 nm to 800 nm to determine its band gap properties. X-ray photoelectron spectroscopy (XPS) analysis was carried out using Omicron Nanotechnology ESCA-14 instrument containing a monochromatic beam of Al-K_{α} radiation source that was used to confirm the chemical composition and valence states. The electrochemical measurements were carried out with an electrochemical workstation (CHI 660B, CH instruments, Austin, TX, USA), containing a typical three electrode system involving platinum wire as the counter electrode, Ag/AgCl (immersed in 3.0 M saturated KCl solution with a potential of E = + 0.210 V Vs SHE) as the reference electrode, and the electroactive material coated glassy carbon electrode (GCE) as the working electrode was used for cyclic voltammetry (CV), galvanostatic charge/discharge (GCD) or chronopotentiometry, and electrochemical impedance spectroscopy (EIS) measurements. An aqueous solution of 1.0 M KOH was used as the electrolyte. From the discharge profile in GCD curves, the specific capacitance, C_S (F g^{-1}) of the MoS_2 nanosheets and MoS_2/ZSO nanocomposites was calculated by using the following relation (1):

$$C_S = \frac{I \times \Delta t}{m \times \Delta V} \ldots\ldots\ldots\ldots (1)$$

Where Δt is the discharge time in sec (s); I is the applied current in amperes (A), m is the mass of active material deposited on GCE in grams (g); ΔV is the discharge potential window applied in volts (V), respectively.

3. Results and Discussion

3.1. Structural Analysis

The structural properties of MoS_2 and MoS_2/ZSO nanocomposites were determined by XRD patterns displayed in Fig. 1 (a). The MoS_2 shows three major diffraction peaks corresponding to the (002), (006), and (008) planes, suggesting that the exfoliated MoS_2 nanosheets are well crystallized. All the diffraction peaks could be indexed to the hexagonal crystal structure of MoS_2 (2H-MoS_2, space group P63/*mmc* (194); JCPDS card No. 37-1492). The most intense peak at 2θ = 14.2° corresponding to the (002) crystalline plane of MoS_2, signifies the ordered stacking of the MoS_2 layers [17, 18]. In the case of nanocomposites, the diffraction peaks corresponding to tetragonal crystal-structured $ZnSb_2O_6$ phase were observed (JCPDS card No. 38-0453) [19]. In contrast, the diffraction planes of MoS_2 were not observed in the XRD patterns of nanocomposites, which suggest the absence of stacking, thus, the exfoliated MoS_2 should be an aggregate of single or few-layered structures [20-22]. The formation of few-layered structures is owing to the incorporation of ZSO nanorods between two adjacent MoS_2 layers, which prevents the stacking effects. Hence, the XRD patterns confirmed the formation of nanocomposites and ordered stacking.
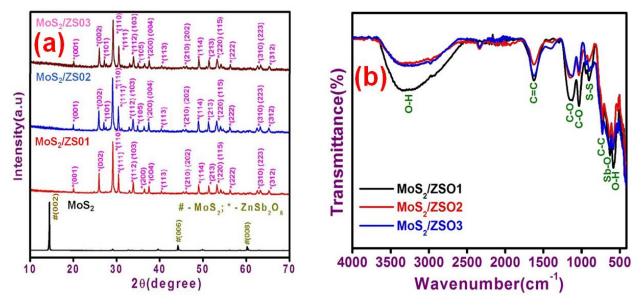

Fig. 1 (a) XRD patterns of MoS_2 nanosheets and MoS_2/ZSO nanocomposites and (b) FT-IR spectra of MoS_2/ZSO nanocomposites.

Figure 1 (b) exhibits the FT-IR spectra of MoS_2/ZSO nanocomposites. The broad peak noticed at 3286 cm^{-1} and a small peak observed at 575 cm^{-1} is attributed to the stretching and out-of-plane bending vibrations of O-H groups. The peak centered at 1620 cm^{-1} corresponds to the

stretching vibrations of C=C groups. The peaks observed at 1130 cm^{-1} and 1028 cm^{-1} are assigned to stretching vibrations of C-O groups. The peak noticed at 900 cm^{-1} can be attributed to the S-S bond. The peak corresponding to skeletal C-C vibrations was centered at 723 cm^{-1}. The peak corresponding to the stretching vibrations of Sb-O is centered at 630 cm^{-1} while the stretching vibrations of Zn-O and Mo-S bands were both centered at 480 cm^{-1}. From the FT-IR spectra, it is evident that the vibrational peaks corresponding to MoS_2 and $ZnSb_2O_6$ phases are present. Moreover, concentrating on the vibrational peak of S-S bond centered at 900 cm^{-1}, the kind of interaction can be understood. The S-S bond is slightly shifted to lower wavenumber in the case of MoS_2/ZSO2 and MoS_2/ZSO3 samples than MoS_2/ZSO1, which means the synergistic interaction between the two nanostructures gets enhanced.

3.2. Morphological Analysis

FE-SEM micrographs of MoS_2 nanostructures are exhibited in Figs. 2 (a) and (b) that represent the plate-like nanosheet morphology. Furthermore, it evidently confirmed that the exfoliation of MoS_2 nanosheets has occurred through the probe assisted ultrasonication strategy. Figure 2 (c) displays the FE-SEM micrograph of MoS_2/ZSO1 sample, in which the $ZnSb_2O_6$ nanorods were randomly distributed on the MoS_2 nanosheets, while the MoS_2/ZSO2 sample exhibited in Fig. 2 (d) showed more number of $ZnSb_2O_6$ nanorods on and in between the MoS_2 nanosheets. Additionally, it is evident that $ZnSb_2O_6$ nanorods have participated in separating or preventing each nanosheet from restacking effects. This can be beneficial for electrolyte ion to diffuse between the nanosheets and access the active surface area possessed by both nanosheets and nanorods. Figure 2 (e) exhibits the FE-SEM micrograph of MoS_2/ZSO3 sample, in which more number of MoS_2 nanosheets were observed than ZSO nanorods. Moreover, these kinds of samples can exhibit significant influence in electrochemical phenomena.

Figure 3 (a) displays HR-TEM micrograph of MoS_2 nanosheets, in which the nanosheets were well separated from each other, confirming the formation of few-layered structures of MoS_2. Figure 3 (b) provides the corresponding SAED pattern, which confirmed the crystalline nature of MoS_2 nanosheets. Figure 3 (c) represents the HR-TEM micrograph of MoS_2/ZSO1 nanocomposites, in which a nanorod was distributed in between two MoS_2 nanosheets and it can be beneficial for better and unique electrochemical properties. The formation of this hierarchical nanostructure is owing to the ultrasonication-assisted magnetic stirring approach. Figure 3 (d)

provides the corresponding SAED pattern, which confirmed the crystalline nature of MoS_2/ZSO1 nanocomposites.
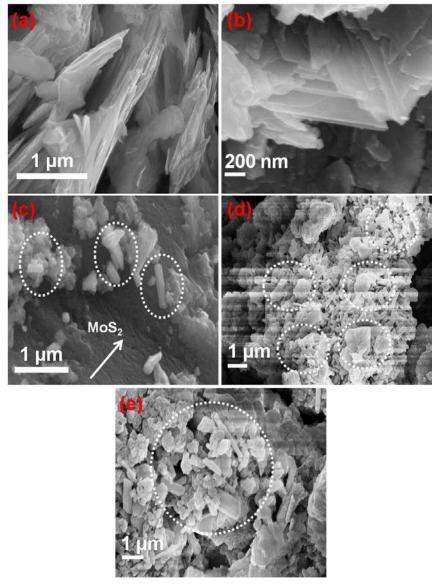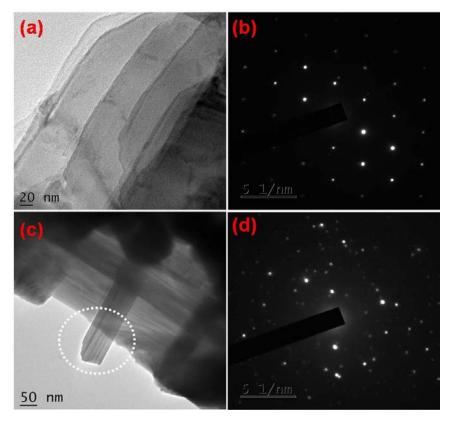

Fig. 2 FE-SEM micrographs of (a) and (b) MoS_2 nanosheets (c) MoS_2/ZSO1 nanocomposites (white dotted rings indicate ZSO nanorods) (d) MoS_2/ZSO2 nanocomposites (white dotted rings indicate presence of ZSO nanorods between MoS_2 nanosheets) and (e) MoS_2/ZSO3 nanocomposites (white dotted ring indicate presence of less number of ZSO nanorods between MoS_2 nanosheets).

Fig. 3 (a) HR-TEM micrograph of MoS_2 nanosheets (b) corresponding SAED pattern (c) HR-TEM micrograph of MoS_2/ZSO nanocomposites and (d) corresponding SAED pattern.

3.3. Optical Analysis

Figure 4 (a) displays the reflectance spectra of MoS_2 nanosheets and MoS_2/ZSO nanocomposites. In the case of MoS_2 nanosheets, the spectra exhibit the onset of broad absorption from 400 nm to 1200 nm. While in the case of MoS_2/ZSO nanocomposites, the absorption intensity gets reduced and can be attributed to the synergistic interaction between the two nanostructures. The band gap values of MoS_2 nanosheets and MoS_2/ZSO nanocomposites were determined using the Kubelka-Munk (K-M) absorption plot as shown in Fig. 4 (b). In order to determine the band gap of MoS_2 nanosheets and MoS_2/ZSO nanocomposites precisely, the K-M plot was magnified and exhibited in Fig. 4 (c). The optical band gap values were found to be 2.64 eV, 2.38 eV, 2.49 eV, and 2.47 eV for MoS_2, MoS_2/ZSO1, MoS_2/ZSO2, and MoS_2/ZSO3 samples, respectively. The decreased band gap value compared to MoS_2 nanosheets is attributable to the formation of heterojunction [23]. Furthermore, it evidently proves that there is synergistic interaction or coordination between MoS_2 and $ZnSb_2O_6$ nanostructures.
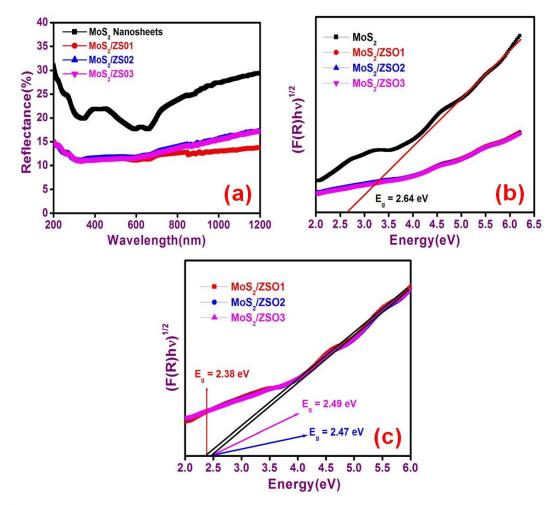
Fig. 4 (a) UV-DRS spectra (b) Corresponding Kubelka-Munk plot and (c) Magnified Kubelka-Munk plot of MoS_2 nanosheets and MoS_2/ZSO nanocomposites.

3.4. Compositional Analysis

Figure 5 (a) exhibits the survey scan XPS spectra of MoS_2 nanosheets. From the survey scan spectral results, it is evident that MoS_2 is composed of only C, Mo, S, and O photoelectron lines. Whereas, the XPS survey scan of MoS_2/ZSO nanocomposites shown in Fig. 5 (b) comprises only C, Mo, S, Zn, Sb, and O photoelectron lines and show no evidence of photoelectron lines of any other impurities. Furthermore, the high-resolution (HR) spectra were recorded for Mo, S, and Sb elements to corroborate the interaction between two different nanostructures and to determine their valence states. Figure 5 (c) represents the HR spectra of Mo $3d$, in which the MoS_2 nanosheets consist of $3d_{3/2}$ and $3d_{5/2}$ transitions at 232.5 eV and 229.3 eV, respectively, corresponding to tetravalent (4+) state of Mo [15]. In the case of nanocomposites the Mo $3d_{3/2}$ and Mo $3d_{5/2}$ transitions were suppressed, which might be ascribed to the synergistic interaction of MoS_2 and

ZSO nanostructures. Figure 5 (d) represents the HR spectra of S $2p$, in which the bare sample exhibits S $2p_{1/2}$ and S $2p_{3/2}$ transitions at 163.3 eV and 162.1 eV, corresponding to S^{2-} state [15]. Meanwhile, in the case of nanocomposites, S $2p_{1/2}$ and S $2p_{3/2}$ transitions were suppressed similar to Mo $3d$ transitions.
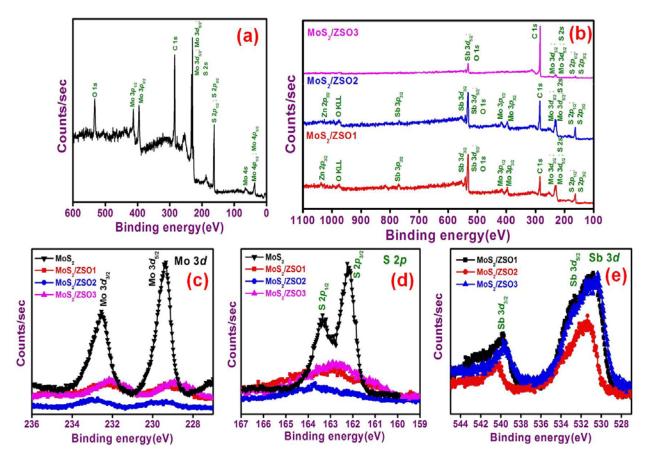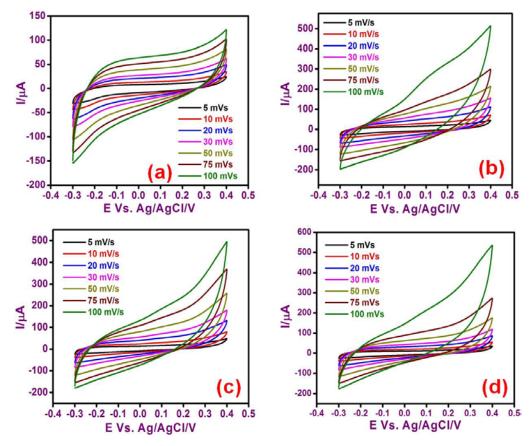

Fig. 5 (a) XPS survey scan spectra of MoS_2 nanosheets (b) XPS survey scan spectra of MoS_2/ZSO nanocomposites (c) HR spectra of Mo $3d$ (d) HR spectra of S $2p$ and (e) HR spectra of Sb $3d$.

In addition, the synergistic effects are confirmed through recording HR spectra of Sb $3d$, as shown in Fig. 5 (e). The Sb $3d_{3/2}$ and Sb $3d_{5/2}$ transitions were observed at 539.8 eV and 530.7 eV (MoS_2/ZSO1), 540.4 eV and 531.3 eV (MoS_2/ZSO2), and 539.7 eV and 530.6 eV (MoS_2/ZSO3), respectively. In all samples, the spin-orbit splitting energy of Sb $3d$ was around 9.1 eV, which evidently confirmed the existence of Sb in pentavalent (5+) state. Meanwhile, the Sb $3d$ photoelectron lines did not get suppressed but show significant shifting in the binding energy

values, which enumerates the synergistic interaction between two nanostructures. Hence, from XPS studies, it is evident that ZSO nanorods have coordinated chemically with MoS_2 nanosheets.
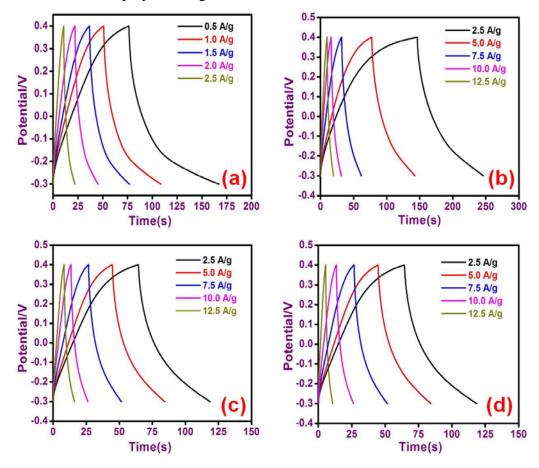
3.5. Electrochemical Analysis

To investigate the electrochemical performance of MoS_2 nanosheets and MoS_2/ZSO nanocomposites, the electrochemical measurements were conducted in 1.0 M KOH electrolyte. The CV curves of MoS_2 nanosheets at various scan rates are shown in Fig. 6 (a), exhibiting EDLC-type behavior [24] with similar shape within the voltage range of −0.3 V to +0.4 V. As a result, it indicates that the specific capacitance is mostly attributed to the rapid and reversible electrochemical reactions. In addition, the current response of the MoS_2 electrode increase gradually with increasing scan rate, indicating excellent reversibility taking place at the electrode material interface.

Fig. 6 CV curves of (a) MoS_2 nanosheets (b) MoS_2/ZSO1 (c) MoS_2/ZSO2 and (d) MoS_2/ZSO3 nanocomposites at different scan rates in 1.0 M KOH electrolyte.

Figures 6 (b-d) exhibit CV curves of MoS$_2$/ZSO nanocomposites at various scan rates. All the CV curves showed distortion in shape compared to CV curves of bare MoS$_2$, which is ascribed to the pseudocapacitive-type phenomena. The occurrence of pseudocapacitive phenomena in MoS$_2$ nanocomposites is owed to the presence of ZSO nanorods. Moreover, in all the MoS$_2$/ZSO nanocomposite samples, the CV curves indicated excellent reversibility, symmetric and capacitive behavior. In addition, the GCD curves of bare-MoS$_2$ nanosheets and MoS$_2$/ZSO nanocomposites were recorded and are displayed in Fig. 7.

Fig. 7 GCD curves of (a) MoS$_2$ nanosheets (b) MoS$_2$/ZSO1 (c) MoS$_2$/ZSO2 and (d) MoS$_2$/ZSO3 nanocomposites at different current densities in 1.0 M KOH electrolyte.

The charge-discharge profile of bare MoS$_2$ nanosheets at different current densities showed typical triangular shape of EDLC characteristics. Meanwhile, the charge-discharge profile of MoS$_2$/ZSO nanocomposites recorded at different current densities also exhibited EDLC-type characteristics with gradual changes in the discharging time at different current densities. This gradual change is due to the addition of ZSO nanorods into MoS$_2$ nanosheets. The discharging

time is comparatively higher in the case of MoS_2/ZSO1 sample than MoS_2/ZSO2 and MoS_2/ZSO3 samples. The reason behind higher discharging time in the case of MoS_2/ZSO1 sample can be attributable to the formation of few-layered structures of MoS_2 without restacking effects. Furthermore, presence of sufficient amount of ZSO nanorods at particular sites of nanosheets helps in prevention of restacking of nanosheets. In the case of MoS_2/ZSO2 and MoS_2/ZSO3 samples, aggregation of ZSO nanorods and restacking of nanosheets can occur, which might be the reason for less discharging time compared to MoS_2/ZSO1 sample.
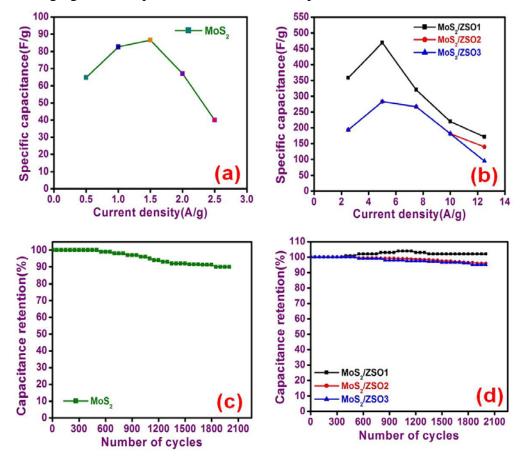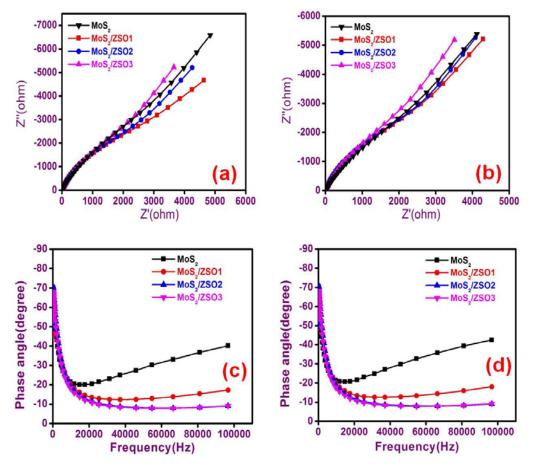

Fig. 8 (a) calculated specific capacitance of MoS_2 nanosheets (b) calculated specific capacitance of MoS_2/ZSO nanocomposites (c) and (d) capacitance retention measurements of MoS_2 nanosheets and MoS_2/ZSO nanocomposites.

The maximum specific capacitance attained was 86.57 F g^{-1} at a current density of 1.5 A g^{-1} for MoS_2 nanosheets (Fig. 8 (a)). Meanwhile, the maximum specific capacitance attained for MoS_2/ZSO nanocomposite electrodes at a current density of 5.0 A g^{-1} was 469.28 F g^{-1} for MoS_2/ZSO1 and 282.85 F g^{-1} for both MoS_2/ZSO2 and MoS_2/ZSO3 electrodes (Fig. 8 (b)).

13

Furthermore, the electrochemical stability of the bare-MoS_2 nanosheets and MoS_2/ZSO nanocomposite electrodes was evaluated to represent their constant electrochemical performance. Electrochemical cycling tests were carried out for 2000 cycles at a current density of 2.0 A g^{-1} for bare-MoS_2 and 10.0 A g^{-1} for MoS_2/ZSO nanocomposites and are exhibited in Figs. 8 (c) and (d).

Fig. 9 Nyquist plots of MoS_2 nanosheets and MoS_2/ZSO nanocomposites (a) before cycling (b) after cycling; Bode plots of MoS_2 nanosheets and MoS_2/ZSO nanocomposites (c) before cycling (d) after cycling.

The maximum capacitance retention of 90.0% was acquired for bare-MoS_2 nanosheets while MoS_2/ZSO nanocomposite electrodes revealed maximum capacitance retention of 102.0%, 96.0%, and 95.0% for MoS_2/ZSO1, MoS_2/ZSO2, and MoS_2/ZSO3 samples, respectively. In the case of MoS_2/ZSO1 sample, in between the cyclic period the capacitance increased up to 104.0%, which means the electrochemical active sites in both MoS_2 nanosheets and ZSO nanorods gets activated and participated in stable electrochemical reactions [25] and also ultrasonication strategy influenced the formation of non-aggregated nanocomposites. In addition, the electrochemical

properties of $ZnSb_2O_6$ nanorods were previously reported with high specific capacitance of 53.3 F g^{-1} with high capacitance retention of 103.5%, and were anticipated to be an active electrode material for supercapacitors [16].

Furthermore, the electrochemical capacitor characteristics of bare-MoS_2 nanosheets and MoS_2/ZSO nanocomposite electrodes were investigated through EIS analysis. Figures 9 (a) and (b) show the Nyquist plots of bare-MoS_2 nanosheets and MoS_2/ZSO nanocomposite electrodes before and after cycling. In all cases, a linear line perpendicular to x-axis at low frequencies was pragmatic, which signifies ideal capacitor characteristics. It is also apparent that all the electrodes exhibit analogous electrochemical phenomena even after cycling, which evidently confirmed the electrochemical stability of bare-MoS_2 nanosheets and MoS_2/ZSO nanocomposite electrodes.

Additionally, Bode plots were measured before and after cycling and are represented in Figs. 9 (c) and (d). The phase angle tends to approach close to $-70°$ at low frequencies in all cases, confirming ideal capacitor behavior and enhanced ion transport rate. The ion transport rate was found to be stable even after complete cycling period, providing evidence of stable electrochemical activity of bare-MoS_2 nanosheets and MoS_2/ZSO nanocomposite electrodes. Hence, from electrochemical studies, it is evident that MoS_2 nanosheets prepared through ultrasonication strategy and MoS_2/ZSO nanocomposites prepared by ultrasonication-assisted homogenous magnetic stirring strategy can be one of the proficient candidates as electrode materials for supercapacitors.

4. Conclusion

In summary, MoS_2 nanosheets were exfoliated through facile sonochemical approach and were composited with ZSO nanorods to investigate their supercapacitor properties. XRD patterns confirmed the formation of composites with 2H-MoS_2 and $ZnSb_2O_6$ phases. Further from FT-IR studies, shifting is observed toward lower wavenumber in S-S bond that elucidates synergistic interaction between the two nanostructures. The FE-SEM and HR-TEM studies revealed the formation of hybrid architectures and crystalline nature. UV-DRS spectra presented the synergistically evolved band gap values of MoS_2/ZSO nanocomposites. XPS investigation confirmed the valence states of the elements present in the nanocomposites and their coordination synergy. The electrochemical studies exhibited better reversibility, symmetric and capacitive nature of bare-MoS_2 nanosheets and MoS_2/ZSO nanocomposites with a maximum specific

capacitance of 469.28 F g^{-1} for MoS$_2$/ZSO1 electrode at a current density of 5.0 A g^{-1}. Electrochemical cycling tests were recorded for 2000 cycles at a current density of 10.0 A g^{-1} and the prepared nanocomposite electrodes exhibited better electrochemical stability with a maximum capacitance retention of 102.0% for MoS$_2$/ZSO1 electrode. These enhanced electrochemical properties are due to the occurrence of synergistic interaction between two different nanostructures, influence of ultrasonication in formation of non-aggregated nanocomposites and existence of more number of electrochemical active sites. Hence, from the results, it is evident that both bare-MoS$_2$ nanosheets and MoS$_2$/ZSO nanocomposites can be one of the electrochemically active electrode materials for supercapacitors.

Acknowledgement

References

[1] T.F. Jaramillo, K.P. Jorgensen, J. Bonde, J.H. Nielsen, S. Horch, and I. Chorkendorff, *Science*, 2007, **317**, 100.

[2] J.Z. Wang, L. Lu, M. Lotya, J.N. Coleman, S.L. Chou, H.K. Liu, Andrew I. Minett, and Jun Chen, *Adv. Energy Mater*., 2013, **3**, 798.

[3] T.M. Masikhwa, M.J. Madito, A. Bello, J.K. Dangbegnon, and N. Manyala, *J. Colloid Interf. Sci*., 2017, **488**, 155.

[4] S.P. Jose, C.S. Tiwary, S. Kosolwattana, P. Raghavan, L.D. Machado, C. Gautam, T. Prasankumar, J. Joyner, S. Ozden, D.S. Galvao, and P.M. Ajayan, *RSC Adv*., 2016, **6**, 93384.

[5] Q.H. Wang, K. Kalantar Zadeh, A. Kis, J.N. Coleman, and M.S. Strano, *Nature Nanotechnol*., 2012, **7**, 699.

[6] C. Zhu, X. Mu, P.P.A. Van, X. Aken, Y. Yu, and J. Maier, *Angew. Chem. Inter. Edn*., 2014, **53**, 2152.

[7] Z. Jian, *Nature comm*., 2014, **5**, 2995.

[8] U. Maitra, U. Gupta, M. De, R. Datta, A. Govindaraj, and C.N. Rao, *Angew. Chem. Int. Ed.*, 2013, **52**, 13057.

[9] T. Zhang, L.B. Kong, M.C. Liu, Y.H. Dai, K. Yan, B. Hu, Yong Chun Luo, and Long Kang, *Mater. Design*, 2016, **112**, 88.

[10] G.F. Ma, H. Peng, J.J. Mu, H.H. Huang, X.Z. Zhou, and Z.Q. Lei, *J. Power Sources*, 2013, **229**, 72.

[11] L.Q. Fan, G.J. Liu, C.Y. Zhang, J.H. Wu, and Y.L. Wei, *International J. Hydrogen Energy*, 2015, **40**, 10150.

[12] Dewei Liang, Zhenfei Tian, Jun Liu, Yixing Ye, Shouliang Wu, Yunyu Cai, and Changhao Liang, *Electrochimica Acta*, 2015, **182**, 376.

[13] Lin Ma, Xiaoping Zhou, Limei Xu, Xuyao Xu, and Lingling Zhang, *NANO: Brief Reports and Reviews*, 2016, **11**, 1650023.

[14] Yukti Arora, Amit P. Shah, Shateesh Battu, Carina B. Maliakkal, Santosh Haram, Arnab Bhattacharya, and Deepa Khushalani, *Scientific Reports*, 2016, **6**, 36294.

[15] Na Li, Hongyang Zhao, Yi Zhang, Zhengqing Liu, Xueyun Gong, and Yaping Du, *CrystEngComm*, 2016, **18**, 4158.

[16] M. Balasubramaniam, and S. Balakumar, *New J. Chem.*, 2018, **42**, 6613.

[17] U.K. Fatema, A.J. Uddin, K. Uemura, and Y. Gotoh, *Textile Research Journal*, 2010, **81**, 659.

[18] S. Najmaei, Z. Liu, P. Ajayan, and J. Lou, *Appl. Phys. Lett.*, 2012, **100**, 01301061.

[19] Jyoti Singh, Neha Bhardwaj, and S. Uma, *Bulletin of Materials Science*, 2013, **36**, 287.

[20] Y. Tian, J. Zhao, W. Fu, Y. Liu, Y. Zhu, and Z. Wang, *Mater. Lett.*, 2005, **59**, 3452.

[21] M.A. Albiter, R. Huirache Acuna, F. Paraguay Delgado, J.L. Rico, and G. Alonso Nunez, *Nanotechnology*, 2006, **17**, 3473.

[22] Y. Tian, Y. He, and Y. Zhu, *Mater. Chem. Phys.*, 2004, **87**, 87.

[23] D. Malwal, and P. Gopinath, *Catal. Sci. Technol.*, 2016, **6**, 4458.

[24] N.S. Choi, Z.H. Chen, S.A. Freunberger, X.L. Ji, Y.K. Sun, K. Amine, G. Yushin, L.F. Nazar, J. Cho, and P.G. Bruce, *Angew. Chem. Int. Ed.*, 2012, **51**, 2.

[25] Kalyanjyoti Deori, Sanjeev Kumar Ujjain, Raj Kishore Sharma, and Sasanka Deka, *ACS Appl. Mater. Interfaces*, 2013, **5**, 10665.